UiT
THE ARCTIC
UNIVERSITY
OF NORWAY

Faculty of Science and Technology, Department of Mathematics and Statistics

Statistical Analysis of Medical Shapes and Directional Data

Jörn Schulz

A dissertation for the degree of Philosophiae Doctor – October 2013

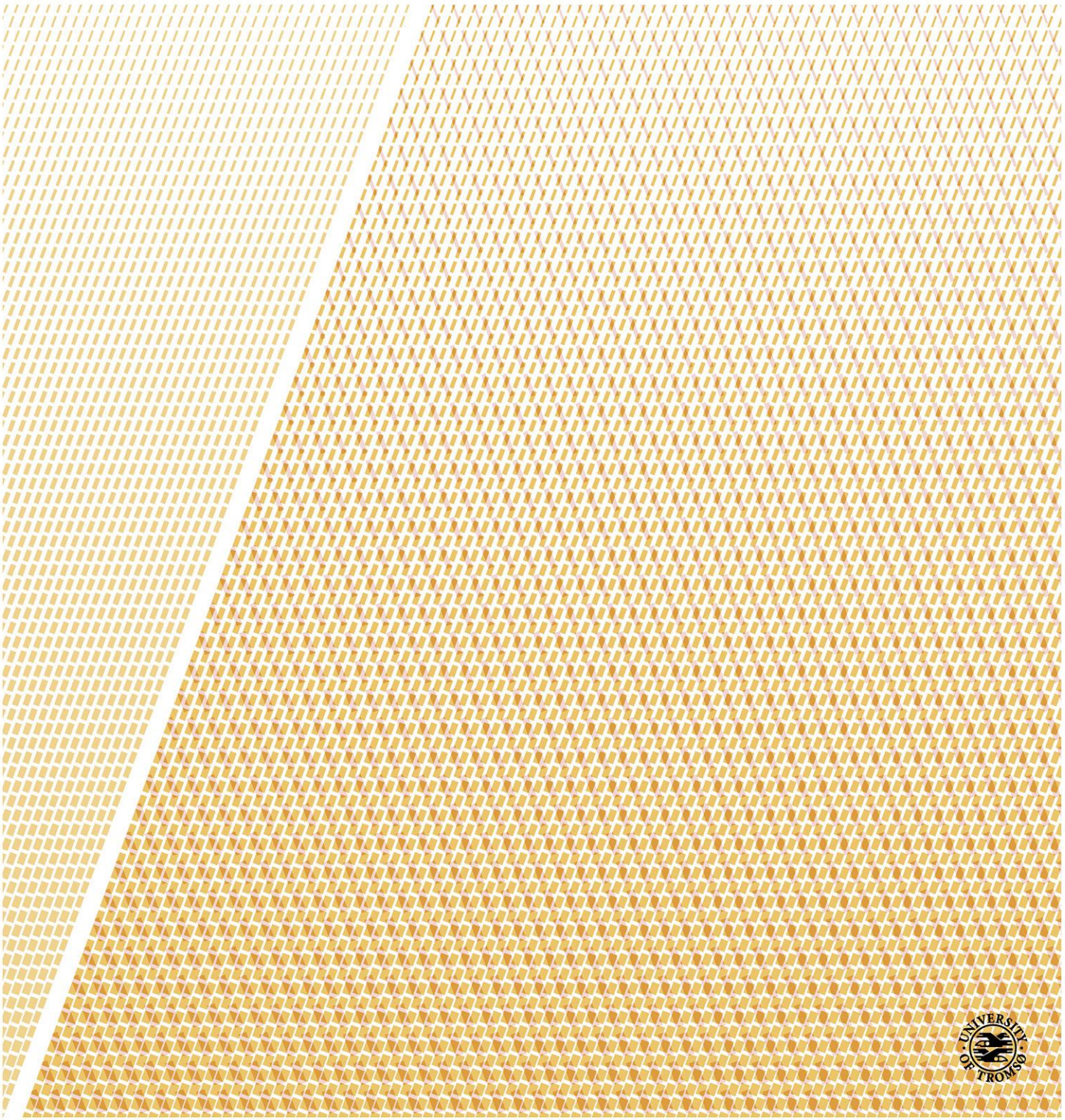

ABSTRACT

The use of statistical shape analysis in medical settings has increased during the last decades. This thesis presents contributions to three major topics of statistical shape analysis. These topics are: the modeling of shape by a geometrical model, the study of rotational shape deformations and the comparison of shapes between populations. All methods that are developed in this thesis are applied to medical problems.

Paper I presents a semiautomatic method for prostate segmentation in radiotherapy treatment planning. To facilitate the manual delineation of the prostate in medical images, an intuitive approach is developed for 3D modeling of the prostate by slice-wise best fitting ellipses in each image. The focus is to estimate a mean shape from a set of training data parametrized by the geometrical model. The proposed estimate is initialized by the definition of a few control points in a new patient. All results are compared to manual delineations by physicians with an average percent-volume overlap of 90%. An additional sample study suggests possible time saving effects by the method and illustrates thereby its potential.

Paper II studies rotational deformations of objects. The rotational deformations such as twisting or bending have been observed as the major variations in some medical applications, where the features of the deformed 3D objects are directional data. Models and estimators are proposed for one or the composition of two simple deformations based on the directional features. The proposed method uses a generalized small circle fitting on the unit sphere. Two analyses of 3D object data are presented in detail: one using skeletal representations in medical image analysis as well as one from biomechanical gait analysis of the knee joint.

Paper III investigates shape differences between two populations of medical objects such as the hippocampi of first episode schizophrenics and controls. Shape differences can be quantified by hypothesis tests, as for instance by a permutation test. Several aspects of a sensitive hypothesis test are elaborated, e.g., geometrical model properties that support accurate statistics of populations. A permutation test is developed to test mean differences of two populations. The proposed method is designed for data whose representations include both Euclidean and non-Euclidean elements. By supporting non-Euclidean components such as directions, the proposed hypothesis test is novel in the study of morphological shape differences. Both global and local analyses showed statistically significant differences between the first episode schizophrenics and controls and demonstrated the sensitivity of the method.

ACKNOWLEDGMENTS

The work presented in this thesis was carried out at the Department of Mathematics and Statistics at the Arctic University of Norway (UiT). Financial support was provided by the Norwegian Research Council through eVita program grant no 176872/V30. The research was performed as part of Tromsø Telemedicine Laboratory, funded by the Norwegian Research Council 2007-2014, grant no 174934.

First, I like to thank my main supervisor Professor Fred Godtliebsen at UiT who gave me the opportunity to do a PhD at such a charming place as Tromsø with impressive nature. Thanks for all the support during the years, the helpful discussions and your never-ending optimism. You also supported my two research visits in the USA in February-April 2010 and 2011 which resulted in Paper II and III of this thesis.

Second, I like to thank my co-supervisors, Professor Stephen M. Pizer and Professor Steve Marron at the University of North Caronlina at Chapel Hill (UNC). I am sincerely grateful for all the help, discussion and tutoring. Stephen widened my knowledge about shape modeling and introduced me in the world of skeletal models. Steve discussed with me several interesting problems in the Euclidean and non-Euclidean world and was always available to give me statistical advices. I also gratefully thank Assistant Professor Sungkyu Jung at the University of Pittsburgh. The collaboration with him was always excellent, helpful and resulted in Paper II. In addition, I wish to thank Jared Vicory, Mark Foskey, Gregg Tracton, Julian G. Rosenman and Martin Styner at the UNC and Juan Carlos Prieto at CREATIS - INSA (France). Jared gave me several advices on running Pablo and fitting skeletal models. I also met Professor Stephan Huckeman at the Georg-August-University of Göttingen during my stay at UNC. Thanks for sharing your impressive knowledge in statistics on manifold data.

I would also like to thank my co-supervisors Stein Olav Skrøvseth at the Norwegian Centre for Integrated Care and Telemedicine (NST) and Professor Håvard Rue at the Norwegian University of Science and Technology in Trondheim. Stein Olav was always there for helpful advices and discussions. Håvard was available for discussions during regular visits in Tromsø. Special thanks goes to Veronika Kristine Tømmerås, Kirsten Marienhagen, Jorunn Andrea Skjelvareid and Rune Sylvarnes at the Department of Oncology at University Hospital of North Norway. They provided me with data and adviced me in radiotherapy planning. Furthermore, I would like to express my gratiude to Jan Terje Kvaløy and the whole department of electrical engineering and computer science at the University of Stavanger to welcome me in their friendly and relaxed enviroment after I moved to Stavanger in January 2013.

Also, I would like to thank my colleagues Marc, Kevin, Kristian, Kajsa and Maciel and many others at TTL,UiT and UNC for an excellent research and social enviroment during the PhD. I will

miss the coffee breaks with random discussions or just to sit on the sofa in the lunch room with an incredible view to the mountains.

Last but not least, I wish to send my gratitude to my family in Germany for the support and the patience to keep the fingers crossed about the years. I wish of course also to thank Izumi and all my friends throughout the world for support, to brighten up and enrich my everyday life during the PhD.

Tromsø, October 2013
Jörn Schulz

LIST OF PUBLICATIONS

Paper I A semiautomatic tool for prostate segmentation in radiotherapy treatment planning, **Schulz, Jörn, Skrøvseth, Stein Olav, Tømmerås, Veronika Kristine, Marienhagen, Kirsten and Godtliebsen, Fred**, submitted to *BMC Medical Imaging*

Paper II Analysis of rotational deformations from directional data, **Schulz, Jörn, Jung, Sungkyu, Huckemann, Stephan, Pierrynowski, Michael, Marron, J.S. and Pizer, Stephen M.**, revised and re-submitted to *Journal of Computational and Graphical Statistics*

Paper III Nonlinear hypothesis testing of geometrical object properties of shapes applied to hippocampi, **Schulz, Jörn, Pizer, Stephen M., Marron, J.S. and Godtliebsen, F.**, preprint

CONTENTS

ABSTRACT i

ACKNOWLEDGMENTS iii

LIST OF PUBLICATIONS v

I INTRODUCTION PART 1

LIST OF ABBREVIATIONS 3

1 INTRODUCTION 5

1.1 Shape representation 7

1.2 Shape statistics 9

1.2.1 General definitions 9

1.2.2 Estimation of shape distributions 11

2 RESULTS AND DISCUSSION 13

2.1 Paper I - Prostate segmentation 13

2.2 Paper II - Estimation of rotational deformations 15

2.3 Paper III - Nonlinear hypothesis testing 20

BIBLIOGRAPHY 23

II PAPERS 27

A semiautomatic tool for prostate segmentation in radiotherapy treatment planning . . . 29

Analysis of rotational deformations from directional data 77

Nonlinear hypothesis testing of geometrical object properties of shapes applied to hippocampi 129

Part I

INTRODUCTION PART

LIST OF ABBREVIATIONS

AAM	Active appearance model
ASM	Active shape model
BFE	Best fitting ellipse
CPNS	Composite principal nested spheres
CT	Computed tomography
GOP	Geometrical object property
MCMC	Markov chain Monte Carlo
MR	Magnetic resonance
PCA	Principal component analysis
PGA	Principal geodesic analysis
PDM	Point distribution model
PNS	Principal nested spheres
RT	Radiotherapy treatment
RTF	Rotation twisting folding
S-rep	Skeletal representation

1

INTRODUCTION

Statistical shape analysis has become an important field in medicine. The use of medical imaging techniques has increased during the last decades and so has the workload of physicians to manually segment target objects in patient data, e.g., in surgery and radiotherapy treatment planning. Manual image interpretation is a time-consuming and error-prone task (Davies et al., 2008). Segmentation of objects is one application of statistical shape analysis. In shape analysis, a *shape distribution* is often obtained from a *training set*, i.e., a representative set of examples from an object class. The shape distribution can be represented by a mean and the main modes of variation and used in a Bayesian framework as a prior distribution. This allows segmentation of an object in data with low image information. Cootes et al. (2001) proposed a segmentation approach, *active appearance model* (AAM) that combines shape distribution and image intensities. In addition to segmentation of objects, other applications of shape analysis are: the study of morphological differences of human organs and body structures (Albertson et al., 2003; Styner et al., 2004; Ferrarini et al., 2006), the study of drug effects in epidemiology (McClure et al., 2013) and the study of deformations of anatomical shapes (Joshi et al., 2002; Rivest et al., 2008; Oualkacha and Rivest, 2012).

Shape analysis of an object $\Omega \subset \mathbb{R}^d$ requires a definition of the term 'shape', a *geometric model* $\mathcal{M}$ that parametrizes Ω and suitable statistics which deal with all components of the geometric model. This thesis is focused on three-dimensional objects, i.e., $d = 3$.

Often, the size, location and rotation of an object are not connected to the underlying shape variation. This thesis will follow Kendall (1984), who defines a shape as the geometrical information that remains when the group of similarity transforms (location, scale and rotation) are removed. However, scaling can be an important feature if the underlying research question is to find shape differences between two populations. Dryden and Mardia (1998) introduced the term *size-and-shape* which defines the geometrical information that remains after removing location and rotation. It follows that shape comparison is affected by subjectivity.

With increased use of imaging techniques, the number of geometric models has also grown steadily. The most well-known examples are landmark models (Kendall, 1984; Bookstein, 1986), boundary point distribution models (PDMs) (Cootes et al., 1992; Kurtek et al., 2011) and the family of skeletal models (Blum and Nagel, 1978; Siddiqi and Pizer, 2008; Pizer et al., 2013) as discussed in Section 1.1.

The geometric model $\mathcal{M}$ can live in a product of Euclidean space (e.g., $\mathbb{R}^{3n}$), a product of non-Euclidean spaces (e.g., S^{2m}), or a product of Euclidean and non-Euclidean spaces (e.g.,

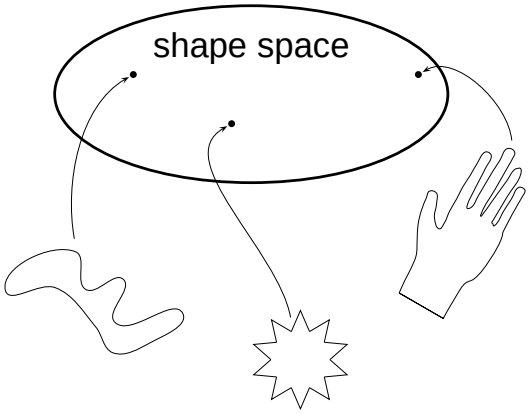

Figure 1: Idea of a shape space. Each object is represented by a point in the shape space.

$\mathbb{R}^{3n} \times S^{2m}$) where n and m depend on the model; $S^d := \{x \in \mathbb{R}^{d+1} : \|x\| = 1\}$ denotes the d-dimensional unit hyper-sphere where $\|x\| := \sqrt{x'x}$ is the Euclidean norm of a column vector $x \in \mathbb{R}^{d+1}$ with transpose x'. The model representation in these coordinate systems reflects a parametrization of an underlying object and is not yet location, rotation and scaling invariant. The *shape space* $\mathcal{S}$ is defined as the space of all possible geometrical configurations of $\mathcal{M}$ which are invariant under global translation, rotation and scaling. Another important notion is the *pre-shape space*, the space of all possible configurations of $\mathcal{M}$ which are invariant under translation and scaling. Dryden and Mardia (1998) have shown that models originally defined in $\mathbb{R}^{3n}$, live on a $(3n-4)$-dimensional unit hyper-sphere S^{3n-4} in the pre-shape space. Thus, given a model $\mathcal{M}$, each shape corresponds to a point in the high-dimensional non-linear shape space $\mathcal{S}$ as depicted in Figure 1. The non-Euclidean data structure requires suitable non-linear statistics.

Multivariate statistics for Euclidean data structures such as *principal component analysis* (PCA) have been intensively developed during the last century. PCA reduces the dimensionality of data and describes the distribution by a selection of eigenvectors, also known as modes of variation. Methods for Euclidean data are not easily applicable to non-Euclidean data. Often, a linear approximation of the non-Euclidean data by an embedding $J : \mathcal{S} \to \mathbb{R}^N$ is applied in order to use classical statistical methods. Huckemann et al. (2010) pointed out that current methods of PCA by linear Euclidean approximation are unsuitable if data in non-linear spaces fall into regions of high curvature, or if they have a large spread. Thus, a generalization of the methods to non-Euclidean data structures is necessary.

The focus of this thesis is the construction and application of geometric models, the use of suitable statistical analyses and the development of novel methods to analyze shapes of objects. In Section 1.1, the most common shape representations will be introduced. Two of these models are used extensively in Paper I-III. In Section 1.2, important definitions and statistical methods will be given that are used particularly in Paper II and Paper III of this thesis. In Section 2, all

three papers are summarized and discussed. The main part of this thesis is Part II which contains the manuscripts of Paper I, II and III, and the corresponding supplementary materials.

1.1 SHAPE REPRESENTATION

First, a geometric model $\mathcal{M}$ is required to parametrize a geometric representation $\Omega \subset \mathbb{R}^3$ where $\mathcal{M}$ typically lies on a manifold. There exists a rich collection of geometrical models in the literature. A selection of important geometrical models are categorized in this thesis as follows:

LANDMARK MODELS A solid object is modeled by the positions of a finite number of mathematical or anatomical landmarks represented by a configuration matrix $\mathbf{X} = (X_1, \ldots, X_K)'$ with K landmarks and $X_i \in \mathbb{R}^3$. The landmark model was introduced by Kendall (1984); Bookstein (1986) who did pioneering work in the field of shape statistics. A problem which arises, is the definition of precise landmarks in order to obtain good correspondence between objects. The definition of landmarks is reasonably intuitive in two-dimensional objects but becomes challenging in three-dimensional objects such as the prostate.

PDM A solid object is defined by the positions of the sampled surface points (Cootes et al., 1992; Kurtek et al., 2011). PDMs are also called pseudo-landmarks and the representation is also given by a configuration matrix $\mathbf{X} \in \mathbb{R}^{3K}$ where K is the number of boundary points. A large number of shape models is based on PDMs.

GEOMETRICAL TEMPLATES The boundary of an object is modeled by a set of parametric geometrical components, such as line segments, triangles, circles and ellipses (Dryden and Mardia, 1998). As a result, an object can be described by a list of geometrical parameters. This approach is used in Paper I of this thesis in order to model the prostate by best-fitting-ellipses (BFEs). The geometrical model is described by parameters $(\theta, \alpha, \phi)' \in (\mathbb{R}^2 \times \mathbb{R}^2_+ \times (-\pi, \pi])^L$ where $\theta^l \in \mathbb{R}^2$ defines the position of the l-ellipse, α^l_1, α^l_2 the length of the first and second principal axis and ϕ the rotation angle as depicted in Figure 2a.

DEFORMATION-OF-ATLAS MODELS The shape changes of an object in an image are modeled by the deformations of a template image provided by an atlas (Pennec, 2008; Zhang et al., 2013). The atlas presents a reference of population of shapes obtained from a set of training shapes. Each template is labeled by a collection of representative features and geometric attributes, e.g., a set of landmarks and parametric geometrical components as previously discussed.

SKELETAL MODELS The idea of skeletal models is based on the *medial locus* of an object, first introduced by Blum and Nagel (1978). The medial locus describes the inherent sym-

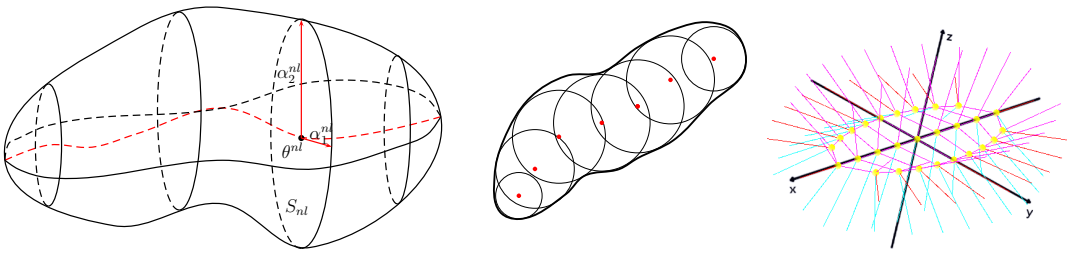

(a) best fitting ellipses (b) medial locus (c) s-rep

Figure 2: Illustration of geometrical models. A geometrical template model of the prostate by slicewise BFEs is visualized in (a). Each ellipse is defined in a slice $l = 1,\ldots,L$ by a position θ^l, the length α_1^l, α_2^l of the 1st and 2nd principal axis, and a rotation angle ϕ. (b) Visualization of points from the medial locus of a two-dimensional object defined by the centers of maximal circles. (c) Discrete skeletal representation (s-rep) of a flat ellipsoid. The skeletal positions are depicted as small spheres. On each side of the sheet, there is a spoke, a vector with direction and length on the top and on the bottom connecting the skeletal sheet to the boundary. Also, for each edge grid point there is an additional spoke vector connecting the skeletal sheet folded to the crest of the slab.

metry of an object. There exist different possibilities to define a medial locus of an object Ω. A formal definition is given by

$$MA_\Omega := \{q \in \mathbb{R}^n \mid |\{p \in \partial\Omega \mid ||q-p|| = d(q,\Omega)\}| > 1\},$$

where $d(q,\Omega) := \min_{p\in\partial\Omega} ||q-p||$ defines the distance of a point $q \in \mathbb{R}^n$ to the object boundary $\partial\Omega$. Figure 2b visualizes points of the medial locus of a two-dimensional object. In 3D, the medial locus is given by the centers of all maximal spheres. A sphere $S \subseteq \Omega$ is called maximal if there exists no larger sphere $\widetilde{S} \subseteq \Omega$ with $S \subset \widetilde{S}$. In Section 3 of Siddiqi and Pizer (2008) it is shown that the medial locus can be described by an inward "grassfire" that starts at the boundary and dies out at a folded version of the medial locus called M_Ω. Given a folded medial locus M_Ω, the medial representation of an object Ω is determined by a set of spoke directions from points of M_Ω to the corresponding points of tangency on the boundary $\partial\Omega$.

Strictly medial representations are limited by the fact that every protruding boundary kink results in additional medial branches. Thus, two versions of the same object with small noise can have drastically different medial representations. Skeletal models achieve additional stability by relaxing the medial constraint. Figure 2c visualizes a discrete version of the skeletal object representation in $\mathbb{R}^3$ composed of a *skeletal sheet* and *spokes* which emanate from a *skeletal position* p_i on the skeletal sheet to the surface. Each spoke is composed of a normal direction u_i with length r_i. The discrete skeletal representation (s-rep) is described by a feature vector $\boldsymbol{s} = (p_1,\ldots,p_{n_a}, r_1,\ldots,r_{n_s}, u_1,\ldots,u_{n_s}) \in \mathbb{R}^{3n_a} \times \mathbb{R}_+^{n_s} \times S^{2n_s}$

with the number n_a of skeletal positions and n_s of skeletal directions. This model and its properties will be discussed and used extensively in Paper III of this thesis. Furthermore, the model is used as an application in Paper II for the study of rotational deformations.

Additional representations are for example implicit models (Leibe et al., 2006) or models using spherical harmonics (Styner et al., 2006).

The calculation of statistics on a set of shapes requires quantification of shape differences. A central difficulty is the identification of correspondence between the parameterized shapes. Hufnagel et al. (2009) proposed the use of correspondence probabilities for the case of unstructured point sets such as PDMs. Alternatively, Cates et al. (2007) introduced correspondence by the optimization of a dynamic particle system by starting with few initial points on the surface (called particle) and splitting the particles in each iteration step. The optimal configuration is defined as one in which the entropy of each shape is balanced against the entropy of the ensemble shapes. Skeletal models introduce correspondence by a stable branching structure of the skeletal sheet, in addition to modeling the skeleton as medial as possible (Pizer et al., 2013). This is discussed in detail in Paper III of this thesis. The geometrical template model used in Paper I introduces correspondence by the templates themself in addition to constraints between the geometrical parameters.

Landmark models and PDMs are often analyzed by PCA although Dryden and Mardia (1998) have shown that these models, originally defined in $\mathbb{R}^{3n}$, live on the unit hyper-sphere S^{3n-4} after removing location and scaling. Other models, such as geometrical template and skeletal models live by definition on a product of Euclidean and non-Euclidean spaces. Therefore, statistics should incorporate all elements of these models.

1.2 SHAPE STATISTICS

1.2.1 *General definitions*

The shape space $\mathcal{S}$ of a model $\mathcal{M}$ can often be understood as a *manifold*. A space is called a d-dimensional manifold if every point of $\mathcal{S}$ has a neighborhood to an open subset of $\mathbb{R}^d$, i.e., for every point p of the manifold exists a map $J : U_p \to \mathbb{R}^d$ for an open neighborhood U_p of p (Bronstein et al., 2008). For example, the tangent space $T_c S^d$ at $c \in S^d$, $d \geq 2$ can be parametrized by $\mathbb{R}^d$. Without loss of generality, let c be the $(d+1)$-dimensional vector $c = (0, \ldots, 0, 1)'$. The exponential map $\mathrm{Exp}_c : \mathbb{R}^d \to S^d$ is defined for $v \in \mathbb{R}^d$ by

$$\mathrm{Exp}_c(v) = \left(\frac{v}{\|v\|} \sin \|v\|, \cos \|v\| \right),$$

with a convention of $\mathrm{Exp}_c(0) = c$. The exponential map has an inverse, called the log map, and is denoted by $\mathrm{Log}_c : S^d \to T_c S^d$. Thereby, S^d is a manifold.

In general, there are two views to manifolds. The *extrinsic view* understands the manifold embedded in a Euclidean space. Statistics are calculated in the tangent space on an extrinsic mean. The *intrinsic view* understands the manifold as a topological space by itself. Shape spaces are often described by a product of a real space $\mathbb{R}^n$ and a d-dimensional unit hyper-sphere S^d as shown before (e.g., Section 1.1). Elements from $\mathbb{R}_+$ can be transformed by the logarithm into $\mathbb{R}$. Thus, it is important to understand statistics on S^d.

To work with observations on S^d, a distance measure is required. An intrinsic distance measure is defined by the Riemannian geodesic distance function d_g by the arc length of the shortest great circle segment joining $x, y \in S^d$, and is

$$d_g(x,y) = \arccos(x'y). \tag{1}$$

For a random element X whose domain is S^d, a sensible notion of the mean $\mu(X)$ is defined by a minimizer of the mean squared distance,

$$\mu_g(X) = \operatorname*{argmin}_{x \in S^d} \mathbb{E}\{d_g^2(x,X)\}, \tag{2}$$

often called the geodesic or Fréchet mean (Fréchet, 1948; Karcher, 1977). A useful measure of dispersion is the geodesic variance which is defined as

$$\mathrm{Var}_g(X) = \mathbb{E}\{d_g^2(\mu_g(X),X)\} = \min_{x \in S^d} \mathbb{E}\{d_g^2(x,X)\} \tag{3}$$

provided that $\mu(X)$ exists. Papers II and III use the intrinsic Fréchet mean to analyze components on S^d. The spherical information in Paper I (the rotation angle of the 1st principal axis of an ellipse) is analyzed by an extrinsic mean. In all three papers, the understanding of a rotational motion in the three-dimensional space (3-space) is important.

The axis–angle pair $(c, \phi) \in S^2 \times [0, 2\pi)$ represents a rotation in 3-space, where a vector $x \in \mathbb{R}^3$ is rotated by (c, ϕ) by applying $x \mapsto R(c, \phi)x$ with the matrix

$$R(c,\phi) = I_3 + \sin\phi\,[c]_\times + (1 - \cos\phi)(cc' - I_3). \tag{4}$$

Here, I_3 is the the three-dimensional unit matrix, and the 3×3 matrix $[c]_\times$ is the cross product matrix satisfying $[c]_\times v = c \times v$ for any $v \in \mathbb{R}^3$. The group of rotations is denoted by $SO(3)$ with $R'R = I_3$ for $R \in SO(3)$.

Thereby, a configuration matrix $\mathbf{X} = (X_1, \ldots, X_K)'$ with $X_i \in \mathbb{R}^3$, $i = 1, \ldots, K$ can be aligned by $\mathbf{X} \to sR(c,\phi)(\mathbf{X} - t)$ with a translation vector $t \in \mathbb{R}^3$, a scaling factor $s \in \mathbb{R}_+$ and a rotation

matrix $R \in SO(3)$. The trajectory of a rotation of a direction vector $x \in S^2$ about an axis $c \in S^2$ is a circle, centered at c with radius $r = \arccos(x'c)$, and is denoted by

$$\delta(c,r) = \{x \in S^2 : x'c = \cos(r)\} \subset S^2. \tag{5}$$

Since $\delta(c,r) = \delta(-c,\pi - r)$, we may assume that $r \leq \pi/2$. A circle $\delta(c,r)$ is called a *great circle* or *geodesic* if $r = \pi/2$, and a *small circle* if $r < \pi/2$. These observations are important for the analysis of rotational motion in Paper II, such as global rotation, rotational bending and rotational twisting.

1.2.2 *Estimation of shape distributions*

An important aspect of shape analysis is to describe the variability of a set of objects which are parametrized by a model $\mathcal{M}$. Another aspect is to find a subspace that best represents the variability of the high-dimensional data (dimension reduction). The geometrical parameters of the BFEs in Paper I are modeled by Gaussian distributions as described in Dryden and Mardia (1998). Another powerful method is PCA for Euclidean data or the generalization of PCA to non-Euclidean data.

PCA describes each data point by a mean and a sum of weighted eigenmodes. It is also a dimension reduction method when retaining only the main modes of variation in a data set. PCA of d-dimensional data can be calculated by a *forward* or *backward* approach corresponding to the order in which the dimensions are considered. In a traditional forward approach the mean is estimated as the 0-dimensional affine space (a point), which is the best fitting subspace to the data. Then, PCA is described by increasing the dimension of the best fitting subspace successively

$$0 \to 1 \to \cdots \to d-1.$$

Starting with fitting the best subspace of dimension $d-1$ to the data, PCA can also be carried out in the reverse order by

$$0 \leftarrow 1 \leftarrow \cdots \leftarrow d-1.$$

In non-Euclidean spaces, such as the d-dimensional unit sphere S^d, generalizations of PCA depend on this forward or backward direction. Damon and Marron (2013) have studied this across a variety of contexts, and have shown that backwards subspace fitting is generally more amenable to analysis, because it is equivalent to a simple adding of constraints. Generalizations of PCA for data on S^d are discussed in the following.

Fletcher et al. (2004) proposed a forward generalization of PCA to manifolds called *principal geodesic analysis* (PGA). The first step of PGA is to find a center point of the data by a forward Fréchet mean. Given the Fréchet mean, the next step is to find the best fitting geodesic passing

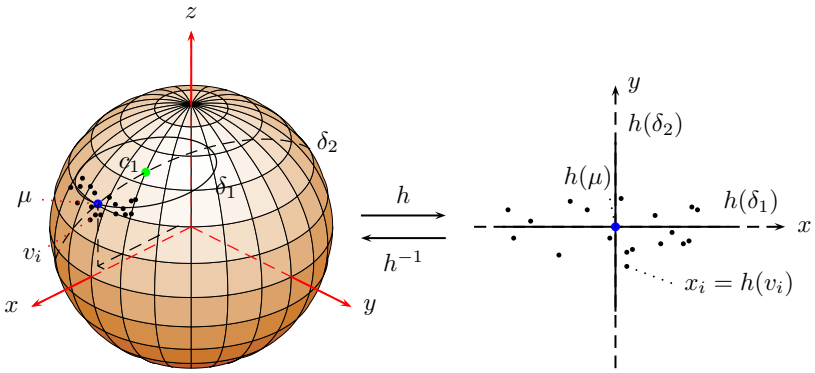

Figure 3: Illustration of point mapping from S^2 to $\mathbb{R}^2$ with PAA. The coordinates $v_i \in S^2$ are mapped to $x_i \in \mathbb{R}^2, i \in \{1,\ldots,n\}$ by a projection h. The coordinate system is defined by the principal circles (δ_1, δ_2). The first principal circle δ_1 is defined by the center c_1 and the radius $r_1 = d_g(c,\mu)$ between the center and the principal circle mean μ. The second principal circle δ_2 is defined by the geodesic passing through the coordinates $(c_1,\mu)^T$. The second principle circle is orthogonal to the first principle circle.

through the mean and afterwards the best fitting geodesic orthogonal to this geodesic. The approach leads to undesirable results if the data are uniformly distributed on a geodesic (e.g., the equator), because the mean would be located at the north or south pole. Huckemann et al. (2010) proposed an important modification to solve this problem by a backward step during the first dimension reduction. Instead of finding the best fitting 0-space (a point), Huckemann proposed to find the best fitting geodesic in the first step. Afterwards, the mean is found on this geodesic, followed by the forward approach of finding the best fitting geodesics through the mean, orthogonal to each other for all dimension $d > 2$. Neither of the methods are suitable for data which are distributed along small circles. This motivates *principal arc analysis* (PAA) by Jung et al. (2011), a generalization of PCA on S^2 by finding the best fit of any circle (small or great) to the data. This approach is illustrated in Figure 3. The first approach discussed above is a classical forward approach, whereas the last two methods contain a backward view to the data in the first step followed by the classical forward view.

Principal nested sphere (PNS) is a fully backward approach that fits the best lower dimensional subsphere in each dimension starting with S^d (Jung et al., 2012). The subspheres can be great or small and thereby, the method includes variation along small and great circles. PNS is described in more detail in Paper III where it is used extensively in order to produce suitable means of shape populations.

2

RESULTS AND DISCUSSION

All three papers in this thesis are motivated by medical applications. Paper I presents a semiautomatic method for prostate segmentation in radiotherapy treatment planning. Paper II presents a novel framework to analyze the biomechanical gait analysis of the knee joint. Paper III presents a novel approach to analyze anatomical shape differences between hippocampi of first episode schizophrenics and controls. Thus, the work in this thesis has demonstrated that statistical shape analysis is an essential approach in medical applications.

2.1 PAPER I - PROSTATE SEGMENTATION

This paper is focused on the development of an intuitively appealing method for the 3D modeling and segmentation of the prostate in radiotherapy treatment (RT) planning of prostate cancer. Prostate cancer is the second most diagnosed cancer worldwide (Jemal et al., 2011). The delineation of the target volume is a time-consuming task that is often performed manually by a physician, slice by slice in a set of computed tomography (CT) or magnetic resonance (MR) images. The proposed semiautomatic method for prostate delineation reduces the workload of physicians and offers comparable accuracy. The method is based on the statistical shape analysis of a training set of prostates that can be understood as the prior information in a Bayesian framework.

The developed geometric model $\mathcal{M}$ of the prostate follows the object parametrization by geometrical templates as proposed in Dryden and Mardia (1998). The prostate has an ellipsoid-like and smooth shape. This motivates modeling the prostate by slicewise BFEs. The BFEs are found by a least-square minimizer as described in Ahn et al. (2001). Suppose the training set consists of N data sets and the prostate is manually outlined in L_n slices in each data set $n = 1,\dots,N$; the stacked ellipses are parametrized by

$$BFE_{nl} := (\theta^{nl}, \alpha^{nl}, \phi^{nl})^T \in \mathbb{R}^2 \times \mathbb{R}^2_+ \times (-\frac{\pi}{2}, \frac{\pi}{2}], l = 1,\dots,L_n, n = 1,\dots,N \tag{6}$$

with positions θ^{nl}, lengths $\alpha_1^{nl}, \alpha_2^{nl}$ of the first and second principal axes, and rotation angles ϕ^{nl} as depicted in Figure 2a. The number of slices L_n usually varies between the data sets $n = 1\dots,N$. Therefore, either an interpolation of the model parameters or an interpolation of the image intensities is necessary. Because the image information of the prostate is low, an interpolation of the image intensities should be avoided. The implemented method assumes to set

manual control points on the boundary which are used to make the BFEs comparable by the transformation of the parametrized ellipses model to a common position, scale and orientation. Control points are assumed in the first, last and center slice. Moreover, the first and second principal axes are reordered, the rotation parameter ϕ^{nl} is relaxed in case of circularity and smoothing is performed between neighboring slices to avoid large forward and backwards rotations. Thereby, correspondence is introduced in the proposed geometric model in Paper I. The normalized parameters result in a mean shape and shape distribution based on the training set. The mean shape is deformed and registered in a new data set based on the control points.

Several approaches are proposed in the literature to segment the prostate. A collection of methods available for prostate segmentation is reviewed by Ghose et al. (2012). The works of Saroul et al. (2008) and Mahdavi et al. (2011) are related to the parametrization method by BFEs as used in Paper I. In contrast to the work of those authors, the approach of slice-wise BFEs introduces more flexibility into the model. Moreover, the method has similarities to a tubular medial representation (Saboo et al., 2009). The proposed approach is very intuitive for physicians; the registration of the mean shape has resulted in fairly accurate estimates in a set of test data with an average volume overlap of 90% compared to the manual segmentations. Moreover, a time saving effect of 30% could be achieved. Thus, the proposed method can provide the physicians with a good initialization of the prostate contour in RT planning. The model fitting procedure for a training data set and the calculation of a mean shape is easy to understand compared to more sophisticated geometric models such as s-reps (Pizer et al., 2013) which support more accurate statistics.

In addition to the deformation and registration of the obtained mean shape in a new data set, the prior was used in a Bayesian framework in order to estimate the posterior shape model in a new data set using a *Markov chain Monte Carlo* (MCMC) method. Only small improvements in the volume overlap could be achieved with large computational costs. This demonstrated the high performance of the mean shape model based on stacked ellipses.

Future work

The small improvements of the segmentation results using MCMC motivates the implementation of an alternative approach, e.g., an *active shape model* (ASM) or an AAM (Cootes et al., 2001; Davies et al., 2008; Heimann, 2008). ASM and AAM model the image intensity variation in addition to the shape variation derived from a training data set. Both shape and image intensity variation are combined in a single statistical model. The image intensity is sampled near the model edges in ASM whereas all image intensity information which is covered by the target object is used in AAM. Both approaches find the final shape model parameters by a minimization procedure. The implementation of these methods may also reduce manual interaction such as the definition of control points.

Further improvements may be achieved by the incorporation of additional constraint and regularization terms such as the surface curvature. Around the center slice of the prostate, a low surface curvature can be expected and smaller changes of model parameters between neighbor slices. Towards the outer slices of the prostate, larger surface curvature can be expected and also larger changes of model parameters between neighbor slices. Thus, the surface curvature could be used as a weight parameter for the implemented regularization terms.

A larger study would be an important step for the implementation of the proposed method into the clinical praxis. This includes a full integration of the method into the work-flow of physicians during the RT planning.

2.2 PAPER II - ESTIMATION OF ROTATIONAL DEFORMATIONS

Segmentation of 3D objects in medical imaging is one application in statistical shape analysis, another is the study of deformations. The deformations of objects such as organs and anatomical structures can appear in several variants, simple and complex types. An important class is rotational deformations including rigid rotation, bending and twisting of an object. The analysis and understanding of such rotational deformations can be important for an accurate medical treatment and diagnosis. For example, the analysis of biomechanical deformations are crucial for the construction of biomechanical models and the treatment of orthopedic problems (Rivest et al., 2008; Ball and Greiner, 2012). Paper II of this thesis studies the rotational deformations and proposes models and estimators based on the directional features $x \in S^2$ of the deformed objects.

If a K-tuple of $K \geq 2$ direction vectors $\mathbf{x} = (x_1, \ldots, x_K) \in (S^2)^K$ is rotated together about a common axis c, then each of the rotated direction vectors is on a circle $\delta(c, r_j)$ as defined in (5) with common center c but with different radii $r_j = \arccos(c' x_j)$, $j = 1, \ldots, K$. As a results, a collection of concentric circles with a common center c and radii tuple $\mathbf{r} = (r_1, \ldots, r_K) \in [0, \pi/2] \times [0, \pi]^{K-1}$ is obtained by

$$\delta(c, \mathbf{r}) = \{(x_1, \ldots, x_K) \in (S^2)^K : x_j' c = \cos(r_j),\ j = 1, \ldots, K\}. \tag{7}$$

The proposed method in Paper II uses the concentric small circles to analyze the rotational deformations of an object. Based on this idea, a rotation model is proposed by

$$X_j = R(c, \theta_j)\mu_j \oplus \varepsilon_j \quad (j = 1, \ldots, K) \tag{8}$$

for a K-tuple of random direction vectors $\mathbf{X} = (X_1, \ldots, X_K)$, unknown constants $c, \mu_j \in S^2$ and latent random variables $\theta_j \in [-\pi/2, \pi/2)$. The error terms ε_j are assumed to be independently distributed, and the $\oplus$ sign defines a suitable action of the error distribution for observations

on S^2. Estimators are developed for $c, \mathbf{r}, \mu_j$ and the latent variable θ_j. Moreover, this model is extended to hierarchical rotations to model and estimate rotational deformations which consist of two independent deformations, e.g., bending and twisting. The numerical performance of the proposed estimator is demonstrated by a simulation study for different situations. Furthermore, the methods are applied to rotationally deformed ellipsoids represented by s-reps as discussed in Section 1.1. This is of interest because several organs have an ellipsoid-like shape such as the prostate. Finally, an analysis of biomechanical data of the knee joint is presented and demonstrates the quality of the method.

Future work

The method introduced in Paper II is an initial work in the analysis of rotational deformations from directional data and opens several potential work directions. The extension of the proposed models to time series models can be investigated in the future. Time series models such as autoregressive-moving-average models could model more accurate rotational deformations observed over time. Furthermore, an improvement of the prediction of θ_j is of interest. The estimations of rotational deformations from s-reps have indicated that it is necessary to incorporate the surface curvature into the model in order to obtain accurate predictions. The Gaussian curvature, mean curvature and shape operator may be useful descriptors (Gray, 1998; Kühnel, 2006). Other research topics would be the extension of the hierarchical deformations to more than two rotational deformations in addition to the incorporation of locational information to the analysis of directional data.

The next two sections present an alternative approach to estimate rotational deformations and an exploratory tool to discriminate rotational deformations. The methodologies presented here, are suggestions for future research.

Analysis of rotational deformations by intersecting geodesics

In Paper II, the estimation of a rotation axis $c \in S^2$ is based on the Fréchet mean of the rotation axes of a set of small circles. Instead of using small circles, an alternative estimator could be based on intersecting geodesics (large circles). Suppose, we have K direction vectors $x_{ij} \in S^2$ at time points $i = 1,2$ with $j = 1,\ldots,K$. An estimation of the rotation axis can be obtained from the intersection of geodesics defined by the pairs (v_i, c_i) with

$$v_j = \frac{x_{1j} + x_{2j}}{||x_{1j} + x_{2j}||} \quad \perp \quad c_j = \frac{x_{1j} \times x_{2j}}{||x_{1j} \times x_{2j}||}, \quad j = 1,\ldots,K. \tag{9}$$

Here, v_j is the bisector of the pair (x_{1j}, x_{2j}). Notice, that the intersection points of two geodesics are perpendicular on S^2. Figure 4 visualizes the intersecting geodesics of 8 directions which are

bent and rigidly rotated around the common rotation axis $c = (1,0,0)'$. It can be observed that the intersection points cluster around the true rotation axis.

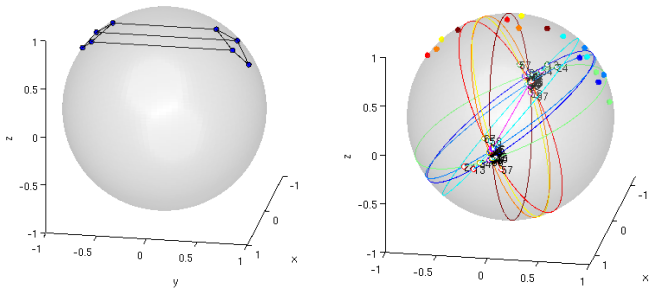

(a) $i = 1$ (b) $i = 1,2$

Figure 4: Toy example. (a) Visualization of 8 observed direction vectors on S^2. (b) Visualization of the directions before and after the rotational deformation. Each color belongs to a direction $j = 1,\ldots,8$, i.e., each color appears three times (two points and the corresponding geodesic). The intersecting geodesics clustering around the true rotation axis $c = (1,0,0)'$.

This idea is an interesting alternative to the proposed approach in Paper II. However, simulations have shown more accurate and robust results using concentric small circles because in certain situations undesirable side-clusters were observed using intersecting geodesics, e.g., in case of observations close to the underlying rotation axis.

An exploratory discrimination tool for rotational deformations

In the following section, a representation called *rotation twisting folding* (RTF) is proposed. RTF compares pairwise directions between different observations to discriminate rotational deformations in rigid rotation, bending and twisting. The RTF representation is designed to capture rotation, bending and twisting by a set of parameters. Thereby, the representation allows to distinguish between the three different types of rotational motions. In particular, specific patterns in the scatterplots of the RTF parameters can be observed.

Suppose, we observe a tuple of directions before rotation (x_{11}, x_{12}) and after rotation (x_{21}, x_{22}), i.e., directions $x_{ij} \in S^2$ with $j = 1,2$ number of directions at time points $i = 1,2$. The RTF representation of (x_{i1}, x_{i2}) is defined by a triple $(\psi, \theta, \tau) \in S^2 \times S^1 \times \mathbb{R}^+$ where ψ indicates the amount of rigid rotation, θ indicates the amount of twisting and τ the amount of bending as visualized in Figure 5 and explained in more detail in the following.

The bisector between the tuple (x_{i1}, x_{i2}) is given by

$$c_i = \frac{x_{i1} + x_{i2}}{||x_{i1} + x_{i2}||}, \quad i = 1,2.$$

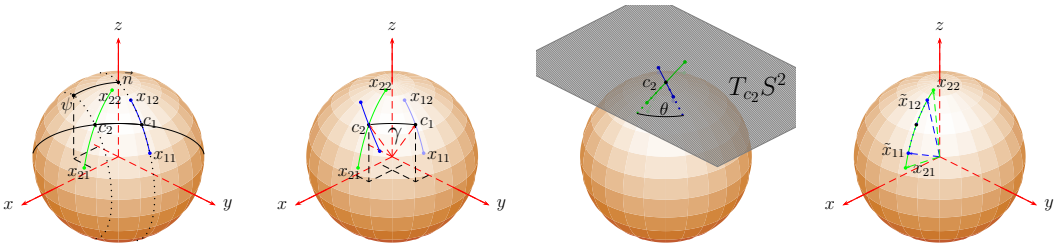

(a) Definition of ψ (b) Definition of γ (c) Definition of θ (d) Definition of τ

Figure 5: Parameter definition in the RTF representation. (a) Definition of $\psi \in S^2$ which defines the rotation direction and rotation angle of bisector c_1 to c_2. (b) Location of the tuple (x_{11}, x_{12}) after rotation corresponding to ψ with rotation angle $\gamma = \arccos(\psi_3)$. (c) Definition of θ by the signed cosinus between the vectors $\mathrm{Log}_{c_2}(\widetilde{R}(c_1,c_2)x_{11})$ and $\mathrm{Log}_{c_2}(x_{21})$ in the tangential plane $T_{c_2}S^2$. (d) Definition of τ by the ratio of the geodesic distances of the tuples (x_{11}, x_{12}) and (x_{21}, x_{22}). Here, $(\tilde{x}_{11}, \tilde{x}_{12})$ is the tuple (x_{11}, x_{12}) after transformation by ψ and θ.

For convenience, denote by $\widetilde{R}(a,b) \in SO(3)$ a rotation matrix that moves $a \in S^2$ to $b \in S^2$, and $\vec{n} = (0,0,1)$ defines the north pole on S^2. Thereby, the direction vector $\psi = (\psi_x, \psi_y, \psi_z) \in S^2$ is defined by

$$\psi := \widetilde{R}(c_1, \vec{n})c_2 \tag{10}$$

which rotates the bisector c_1 to c_2 with rotation angle $\gamma = \arccos(\psi_z)$. The direction $\psi \in S^2$ indicates the amount of rigid rotation. The ratio of the two pairs of directional vectors is defined by

$$\tau := \frac{d_g(x_{21}, x_{22})}{d_g(x_{11}, x_{12})} \tag{11}$$

with the geodesic distance d_g as defined in (1). The ratio τ indicates the amount of bending between the observations with $\tau = 1$ in case of no bending. Finally, x_{11} is mapped to $\kappa_1 \in \mathbb{R}^2$ by $\kappa_1 = \mathrm{Log}_{c_2}(\widetilde{R}(c_1,c_2)x_{11})$; and x_{21} is mapped to $\kappa_2 \in \mathbb{R}^2$ by $\kappa_2 = \mathrm{Log}_{c_2}(x_{21})$. The vectors κ_1 and κ_2 are elements of the tangent space $T_{c_2}S^2$. Thereby, the parameter θ is defined by

$$\theta := sign(\kappa_1 \times \kappa_2) \arccos\left(\frac{\kappa_1' \kappa_2}{||\kappa_1|| ||\kappa_2||}\right), \tag{12}$$

where $sign(\kappa_1 \times \kappa_2)$ is the sign of the cross product of κ_1 and κ_2. The parameter θ indicates the amount of twisting with $\theta = 0$ in case of no twisting.

The decomposition by the RTF representation can be understood by considering a simple example, see Figure 6. Suppose, an object is modeled by four surface points with attached directions $x_{0j}, j = 1, \ldots, 4$. Moreover, consider 30 random observations after rigid rotation, bending

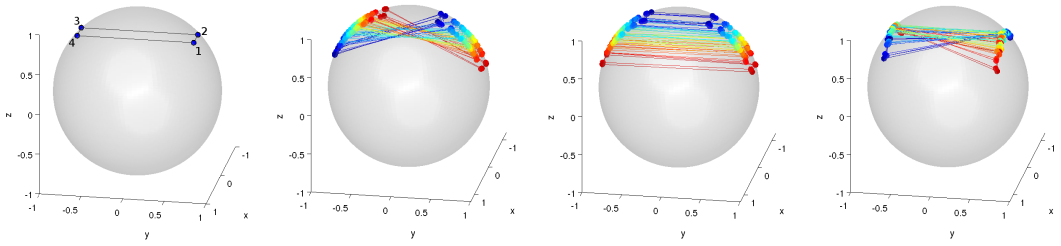

(a) Direction vectors (b) Rigid rotation (c) Bending (d) Twisting

Figure 6: Toy example for the RTF representation. (a) Each direction vector x_{0j} is a point on S^2, $j = 1,\ldots,4$. (b-d) 30 realizations of random rotational deformations. Different colors represent different observations. (b) Rigid rotation about $(1,0,0)'$. (c) Bending reflected by a rotation of the directions on the left and right side of the sphere about the common axis $(1,0,0)'$ by common angle but in opposite directions. (d) Twisting reflected by a rotation of directions on the left and right side about the common axis $(0,1,0)'$ by common angle but in opposite directions.

and twisting of the object as described in Figure 6 where each rotational deformation was generated by

$$X_{ij} = R(\omega,\phi)x_{0j} \oplus \varepsilon \quad \text{or} \quad X_{ij} = R(\omega,-\phi)x_{0j} \oplus \varepsilon$$

with $i = 1,\ldots,30$, $j = 1,\ldots,4$, $\phi \sim N(0,\eta^2)$ and a rotation axis $\omega \in S^2$. The RTF parametrization is calculated between all pairwise combinations $(x_{0k_1}, x_{0k_2}, X_{ik_1}, X_{ik_2})$ with

$$\{k_1,k_2\} \in \{\{1,2\},\{1,3\},\{1,4\},\{2,3\},\{2,4\},\{3,4\}\},$$

represented by the tuples (X_{ik_1}, X_{ik_2}).

The RTF representation for each rotational deformation is visualized in Figure 7. Observations obtained by rigid rotation (Figure 6b) result in a small spread of the parameters θ and τ (Figures 7d and 7g) but in a wide spread of ψ around the underlying rotation axis (Figure 7a). Observations obtained by a bending deformation (Figure 6c) result in a small spread of the parameter θ but in a wide spread of τ (Figures 7e and 7h). The parameter ψ indicates a rigid rotation for the tuples (X_{i1}, X_{i2}) and (X_{i3}, X_{i4}) about $(1,0,0)'$, no rotation for the tuples (X_{i1}, X_{i4}) and (X_{i2}, X_{i3}), and a minor rotation for the tuples (X_{i1}, X_{i3}) and (X_{i2}, X_{i4}) about $(0,0,1)'$ (Figure 7b). Observations obtained by twisting (Figure 6d) result in a small spread of the parameter τ but in a wide spread of θ (Figures 7f and 7i). The parameter ψ indicates only rigid rotation for the tuples (X_{i1}, X_{i2}) and (X_{i3}, X_{i4}) (Figure 7c).

The presented results reveal the potential of the RTF representation as an exploratory tool for the discrimination analysis of rotational deformations from directional data. However, further simulations and research is required on the basis of more complex objects and real data examples.

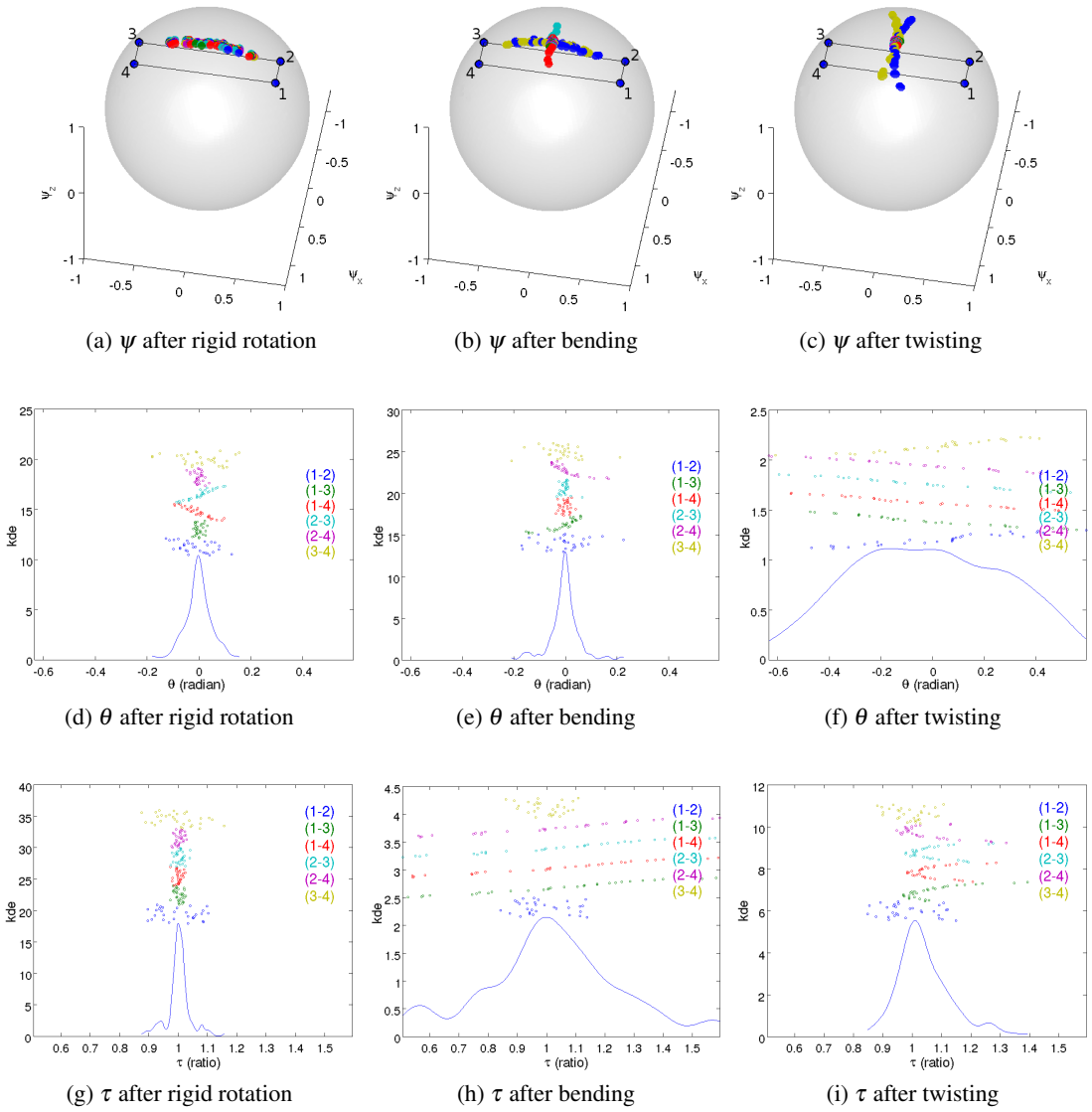

(a) ψ after rigid rotation (b) ψ after bending (c) ψ after twisting

(d) θ after rigid rotation (e) θ after bending (f) θ after twisting

(g) τ after rigid rotation (h) τ after bending (i) τ after twisting

Figure 7: RTF representation of rigid rotated, bent and twisted directions. (a-c) Parameter ψ, (d-f) parameter θ (g-i) parameter τ of the RTF representation. In each plot 180 realizations (points) are depicted of the corresponding RTF parameter. Different colors represent different direction tuples, e.g., (1-2) for the tuple (X_{i1}, X_{i2}) with $i = 1, \ldots, 30$.

The proposed method may be useful for a classification of rotational deformations into rigid rotation, bending and twisting. Such a classification is left for future research.

2.3 PAPER III - NONLINEAR HYPOTHESIS TESTING

Another application of statistical shape analysis is presented in Paper III by exploring shape differences between hippocampi of first episode schizophrenics and controls. The study of mor-

phological changes of human organs and body structures is of general interest in medical analysis, e.g., the understanding of neuroanatomical structures of the human brain (Gerig et al., 2001; Styner et al., 2004; Ferrarini et al., 2006).

Paper III proposes a novel method to test mean differences of populations on data whose representations include both Euclidean and non-Euclidean elements. Several aspects of a sensitive hypothesis test are elaborated such as important geometrical model properties which support accurate statistics of populations. The s-rep model (Pizer et al., 2013) is presented as a suitable model that includes Euclidean components and components which live on spheres. A statistical method based on PNS (Jung et al., 2012) is proposed to calculate means and to analyze the Euclidean and non-Euclidean components of the models. Finally, a permutation test is presented based on Pesarin (2001); Terriberry et al. (2005), in order to test for mean differences. A permutation test is a non-parametric approach that uses the data to estimate the sampling distribution of the test statistic under the null-hypothesis of equal distributions. Because of the assumption that populations have equal distributions, it is valid to permute the data between the populations without affecting the distribution of the test statistic. The test statistic is defined by a difference measure. An appropriate difference measure is presented for the analysis of s-reps. The difference measure quantify the mean difference of geometrical object properties (GOP) which are single or a collection of s-rep features. A global and local test based on the GOP differences are proposed taking into account the problem of multiple comparison correction.

The analysis of first episode schizophrenics compared to controls demonstrated the power of the permutation test, both globally as well as locally. Several statistically significant findings could be made. The global test established a significant shape difference of the hippocampi between schizophrenics and controls. The local test showed a significant loss of hippocampal volume for schizophrenics. The significant volume difference was observed in the x and y-directions but not in the z-direction for the aligned hippocampi. Moreover, several spoke directions were found as statistically significant by the local test. These findings may be of high interest in neuroscience. In addition, Paper III is a novel study that analyzes morphological differences using non-Euclidean data components such as directional information using s-reps. Moreover, a bias for the test results was observed depending on the shape distribution used for the model fitting. The choice of an appropriate shape distribution of a population is discussed in more detail in the paper. Furthermore, the impact of a chosen data pre-processing was discovered.

Future work

Several open questions have been raised during the implementation of the proposed nonlinear hypothesis test. A possible extension of the study is to investigate hippocampal changes of schizophrenics and controls in longitudinal data. Studies such as Narr et al. (2004); Mamah et al. (2012); McClure et al. (2013) have indicated the need for a more sensitive hypothesis test

in order to examine shape differences inside a treatment group over time. A detailed power study on the basis of simulated data and investigation of alternative combining functions for the global test are also left open. Moreover, potential improvements can be made in the data modeling. This includes the incorporation of image intensities in addition to morphological features in order to test for population differences. Furthermore, the fitting procedure of s-reps to the data could be improved in the future, e.g., by an automatic parameter choice for the fitting procedure and an adaptive grid size choice of the skeletal sheet.

BIBLIOGRAPHY

Ahn, S. J., Rauh, W., and Warnecke, H.-J. (2001), "Least-Squares Orthogonal Distances Fitting of Circle, Sphere, Ellipse, Hyperbola, and Parabola," *Pattern Recognition*, 34, 2283–2303.

Albertson, R. C., Streelman, J. T., and Kocher, T. D. (2003), "Genetic Basis of Adaptive Shape Differences in the Cichlid Head," *Journal of Heredity*, 94, 291–301.

Ball, K. A. and Greiner, T. M. (2012), "A Procedure to Refine Joint Kinematic Assessments: Functional Alignment," *Computer Methods in Biomechanics and Biomedical Engineering*, 15, 487–500.

Blum, H. and Nagel, R. (1978), "Shape Description Using Weighted Symmetric Axis Features," *Pattern Recognition*, 10, 167–180.

Bookstein, F. L. (1986), "Size and Shape Spaces for Landmark Data in Two Dimensions," *Statistical Science*, 1, 181–242.

Bronstein, A. M., Bronstein, M. M., and Kimmel, P. (2008), *Numerical Geometry of non-Rigid Shapes*, Heidelberg, Germany: Springer.

Cates, J., Fletcher, P., Styner, M., Shenton, M., and Whitaker, R. (2007), "Shape Modeling and Analysis with Entropy-Based Particle Systems," in *Information Processing in Medical Imaging*, vol. 4584 of *Lecture Notes in Computer Science*, pp. 333–345.

Cootes, T. F., Edwards, G., and Taylor, C. (2001), "Active Appearance Models," *Pattern Analysis and Machine Intelligence, IEEE Transactions on*, 23, 681–685.

Cootes, T. F., Taylor, C., Cooper, D., and Graham, J. (1992), "Training Models of Shape from Sets of Examples," in *Proc. British Machine Vision Conference*, eds. Hogg, D. and Boyle, R., Berlin. Springer-Verlag, pp. 9–18.

Damon, J. and Marron, J. S. (2013), "Backwards Principal Component Analysis and Principal Nested Relations," *Journal of Mathematical Imaging and Vision*, dOI: 10.1007/s10851-013-0463-2.

Davies, R., Twining, C., and Taylor, C. (2008), *Statistical Models of Shape - Optimisation and Evaluation*, London, UK: Springer.

Dryden, I. L. and Mardia, K. V. (1998), *Statistical Shape Analysis*, Chichester, UK: Wiley.

Ferrarini, L., Palm, W. M., Olofsen, H., van Buchem, M. A., Reiber, J. H., Admiraal-Behloul, F., et al. (2006), "Shape Differences of the Brain Ventricles in Alzheimer's Disease," *NeuroImage*, 32, 1060–1069.

Fletcher, P. T., Lu, C., Pizer, S. M., and Joshi, S. (2004), "Principal Geodesic Analysis for the Study of Nonlinear Statistics of Shape," *IEEE Transactions on Medical Imaging*, 23, 995–1005.

Fréchet, M. (1948), "Les Éléments Aléatoires de Nature Quelconque dans un Espace Distancié," *Annales de l'Institut Henri Poincaré*, 10, 215–310.

Gerig, G., Styner, M., Shenton, M. E., and Lieberman, J. A. (2001), "Shape Versus Size: Improved Understanding of the Morphology of Brain Structures," *Medical Image Computing and Computer-Assisted Intervention*, 24–32.

Ghose, S., Oliver, A., Martá, R., Lladó, X., Vilanova, J. C., Freixenet, J., Mitra, J., Sidibé, D., and Meriaudeau, F. (2012), "A Survey of Prostate Segmentation Methodologies in Ultrasound, Magnetic Resonance and Computed Tomography Images," *Computer Methods and Programs in Biomedicine*, 108, 262–287.

Gray, A. (1998), *Modern Differential Geometry of Curves and Surfaces with Mathematica*, Boca Raton, USA: CRC Press, 2nd ed.

Heimann, T. (2008), *Statistical shape models for 3D medical image segmentation*, Saarbrücken, Germany: VDM Verlag Dr. Müller.

Huckemann, S., Hotz, T., and Munk, A. (2010), "Intrinsic Shape Analysis: Geodesic PCA for Riemannian Manifolds modulo Isometric Lie Group Actions," *Statistica Sinica*, 20, 1–58.

Hufnagel, H., Ehrhardt, J., Pennec, X., Ayache, N., and Handels, H. (2009), "Computing of Probabilistic Statistical Shape Models of Organs Optimizing a Global Criterion," *Methods of Information in Medicine*, 48, 314–319.

Jemal, A., Bray, F., Center, M. M., Ferlay, J., Ward, E., and Forman, D. (2011), "Global Cancer Statistics," *CA: A Cancer Journal for Clinicians*, 61, 69–90.

Joshi, S., Pizer, S. M., Fletcher, P., Yushkevich, P., Thall, A., and Marron, J. S. (2002), "Multiscale Deformable Model Segmentation and Statistical Shape Analysis Using Medial Descriptions," *IEEE Transactions on Medical Imaging*, 21, 538–550.

Jung, S., Dryden, I. L., and Marron, J. S. (2012), "Analysis of Principal Nested Spheres," *Biometrika*, 99, 551–568.

Jung, S., Foskey, M., and Marron, J. S. (2011), "Principal Arc Analysis on Direct Product Manifolds," *Annals of Applied Statistics*, 5, 578–603.

Karcher, H. (1977), "Riemannian Center of Mass and Mollifier Smoothing," *Communications on Pure and Applied Mathematics*, 30, 509–541.

Kendall, D. G. (1984), "Shape Manifolds, Procrustean Metrics, and Complex Projective Spaces," *Bulletin of the London Mathematical Society*, 16, 81–121.

Kühnel, W. (2006), *Differential Geometry*, vol. 16 of *Student Mathematical Library*, Wiesbaden, Germany: Friedr. Vieweg & Sohn Verlag, 2nd ed.

Kurtek, S., Ding, Z., Klassen, E., and Srivastava, A. (2011), "Parameterization-Invariant Shape Statistics and Probabilistic Classification of Anatomical Surfaces," in *Information Processing in Medical Imaging*, vol. 22, pp. 147–158.

Leibe, B., Leonardis, A., and Schiele, B. (2006), "An Implicit Shape Model for Combined Object Categorization and Segmentation," in *Toward Category-Level Object Recognition*, Springer Berlin Heidelberg, Lecture Notes in Computer Science, pp. 508–524.

Mahdavi, S. S., Chng, N., Spadinger, I., Morris, W. J., and Salcudean, S. E. (2011), "Semi-Automatic Segmentation for Prostate Interventions," *Medical Image Analysis*, 15, 226–237.

Mamah, D., Harms, M. P., Barch, D. M., Styner, M. A., Lieberman, J., and Wang, L. (2012), "Hippocampal Shape and Volume Changes with Antipsychotics in Early Stage Psychotic Illness," *Frontiers in Psychiatry*, 3, 1–10.

McClure, R. K., Styner, M., Maltbie, E., Liebermann, J. A., Gouttard, S., Gerig, G., Shi, X., Zhu, H., et al. (2013), "Localized Differences in Caudate and Hippocampal Shape are Associated with Schizophrenia but not Antipsychotic Type," *Psychiatry Research: Neuroimaging*, 211, 1–10.

Narr, K. L., Thompson, P. M., Szeszko, P., Robinson, D., Jang, S., Woods, R. P., Kim, S., Hayashi, K. M., Asunction, D., Toga, A. W., and Bilder, R. M. (2004), "Regional Specificity of Hippocampal Volume Reductions in First-Episode Schizophrenia," *NeuroImage*, 21, 1563–1575.

Oualkacha, K. and Rivest, L.-P. (2012), "On the Estimation of an Average Rigid Body Motion," *Biometrika*, 99, 585–598.

Pennec, X. (2008), "Statistical Computing on Manifolds: from Riemannian Geometry to Computational Anatomy," *Emerging Trends in Visual Computing*, 5416, 347–386.

Pesarin, F. (2001), *Multivariate Permutation Tests with Applications to Biostatistics*, Chichester, UK: John Wiley & Sons.

Pizer, S. M., Jung, S., Goswami, D., Zhao, X., Chaudhuri, R., Damon, J. N., Huckemann, S., and Marron, J. S. (2013), "Nested Sphere Statistics of Skeletal Models," in *Innovations for Shape Analysis: Models and Algorithms*, Springer Lecture Notes in Computer Science., pp. 93–115.

Rivest, L.-P., Baillargeon, S., and Pierrynowski, M. (2008), "A Directional Model for the Estimation of the Rotation Axes of the Ankle Joint," *Journal of the American Statistical Association*, 103, 1060–1069.

Saboo, R., Levy, J., Chaney, E., and Pizer, S. M. (2009), "Medial Models of Populations of Nearly Tubular Objects," in *Proceedings of the MICCAI Workshop on Probabilistic Models for Medical Image Analysis*, pp. 232–243.

Saroul, L., Bernard, O., Vray, D., and Friboulet, D. (2008), "Prostate Segmentation in Echographic Images: A Variational Approach Using Deformable Super-Ellipse and Rayleigh Distribution," in *IEEE International Symposium on Biomedical Imaging: From Nano to Macro, ISBI 2008*, pp. 129–132.

Siddiqi, K. and Pizer, S. (2008), *Medial Representations: Mathematics, Algorithms and Applications*, Computational Imaging and Vision, Vol. 37, Dordrecht, Netherlands: Springer, 1st ed.

Styner, M., Lieberman, J., Pantazis, D., and Gerig, G. (2004), "Boundary and Medial Shape Analysis of the Hippocampus in Schizophrenia," *Medical Image Analysis*, 8, 197–203.

Styner, M., Oguz, I., Xu, S., Brechbühler, C., Pantazis, D., Levitt, J., Shenton, M., and Gerig, G. (2006), "Framework for the Statistical Shape Analysis of Brain Structures Using SPHARM-PDM," *The Insight Journal*, 242–250.

Terriberry, T., Joshi, S., and Gerig, G. (2005), "Hypothesis Testing with Nonlinear Shape Models," in *Information Processing in Medical Imaging*, eds. Christensen, G. and Sonka, M., Springer Berlin Heidelberg, vol. 3565 of *Lecture Notes in Computer Science*, pp. 15–26.

Zhang, S., Zhan, Y., Cui, X., Gao, M., Huang, J., and Metaxas, D. (2013), "3D Anatomical Shape Atlas Construction Using Mesh Quality Preserved Deformable Models," *Computer Vision and Image Understanding*, 117, 1061–1071.

Part II

PAPERS

Paper I

A semiautomatic tool for prostate segmentation in radiotherapy treatment planning

Schulz, Jörn, Skrøvseth, Stein Olav, Tømmerås, Veronika Kristine, Marienhagen, Kirsten and Godtliebsen, Fred

submitted to *BMC Medical Imaging*

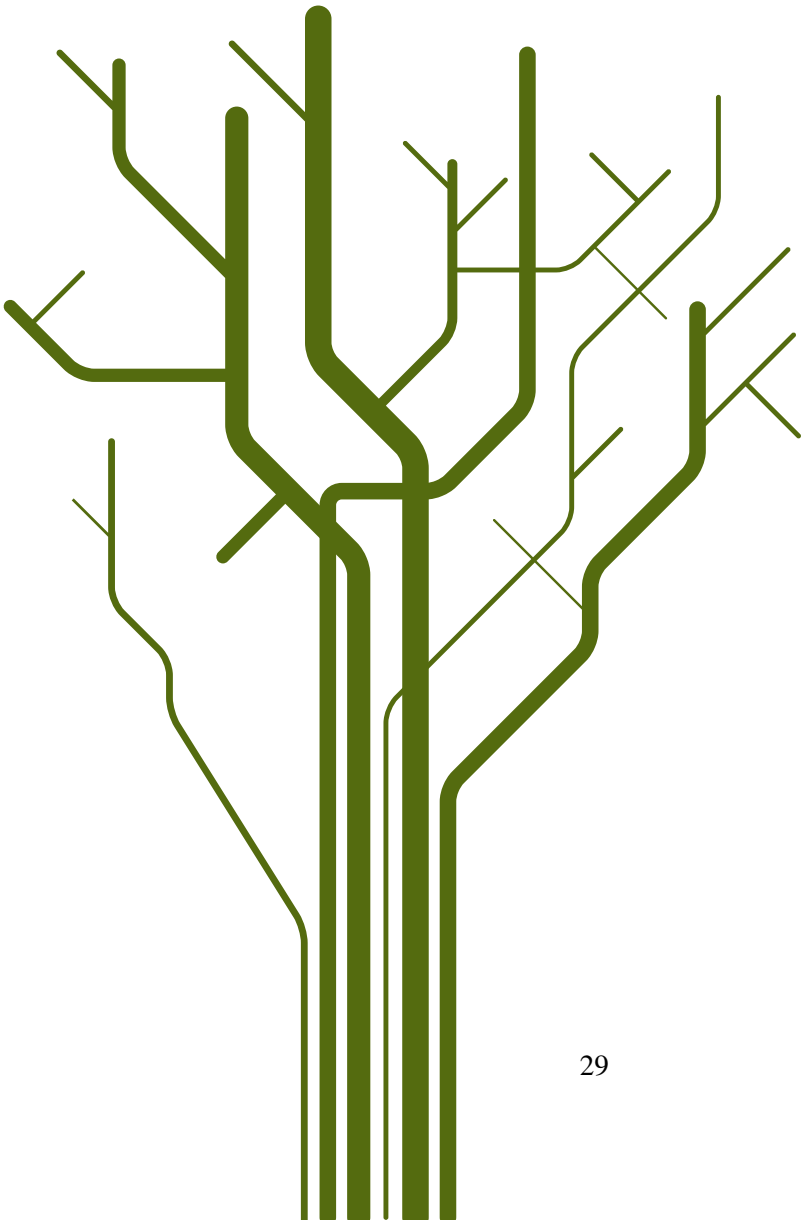

Paper II

Analysis of rotational deformations from directional data

Schulz, Jörn, Jung, Sungkyu, Huckemann, Stephan, Pierrynowski, Michael, Marron, J.S. and Pizer, Stephen M.

revised and re-submitted to *Journal of Computational and Graphical Statistics*

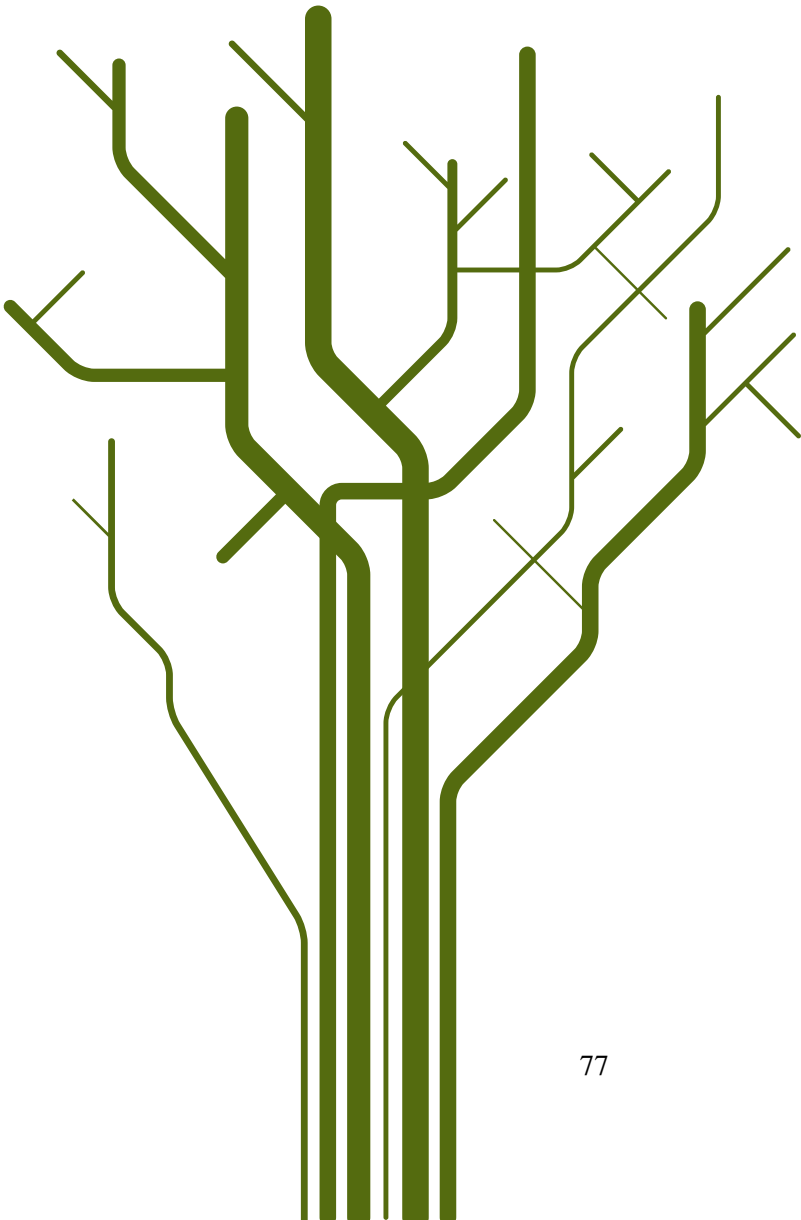

Paper III

Nonlinear hypothesis testing of geometrical object properties of shapes applied to hippocampi

Schulz, Jörn, Pizer, Stephen M., Marron, J.S. and Godtliebsen, F.

preprint

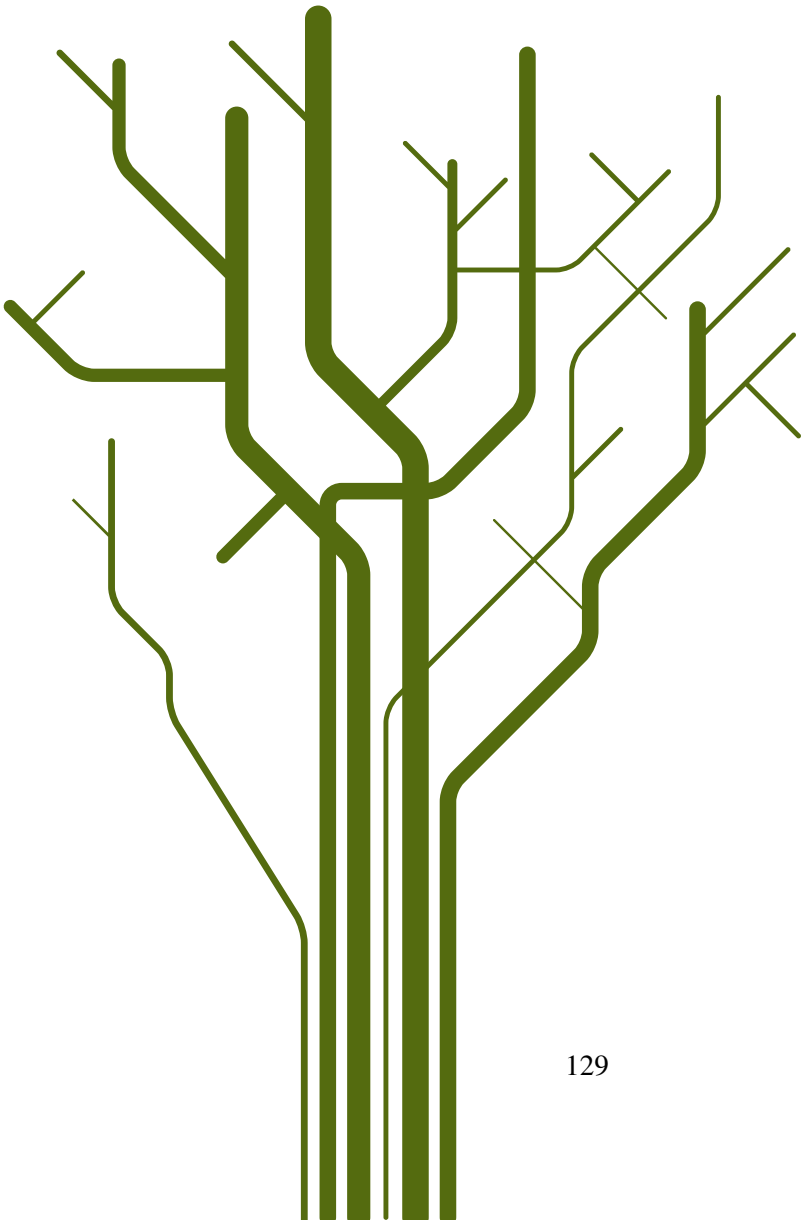

ISBN 978-82-8236-118-7